Water Resources Research

RESEARCH ARTICLE
10.1029/2022WR033514

Toward Large-Scale Soil Moisture Monitoring Using Rail-Based Cosmic Ray Neutron Sensing

Daniel Altdorff[1,2], Sascha E. Oswald[1], Steffen Zacharias[3], Carmen Zengerle[3], Peter Dietrich[3,4], Hannes Mollenhauer[3], Sabine Attinger[1,2], and Martin Schrön[3]

[1]Institute of Environmental Science and Geography, University of Potsdam, Potsdam, German, [2]UFZ Leipzig—Helmholtz Centre for Environmental Research GmbH, Department of Computational Hydrosystems, Leipzig, Germany, [3]Department for Monitoring and Exploration Technologies, UFZ—Helmholtz Centre for Environmental Research GmbH, Leipzig, Germany, [4]Center for Applied Geoscience, University of Tübingen, Tübingen, Germany

Key Points:

- The first rail-borne Cosmic ray neutron sensing system for automatic and continuous soil water content monitoring at the hectare scale is presented
- The system provided almost uninterrupted data from September 2021 to July 2022 along a 9 km railway track in the Harz low mountains, Germany
- Results showed spatial pattern, related to surface features, seasonal change, and individual responses of railway parts to wetting and drying

Correspondence to:
D. Altdorff,
daniel.altdorff@uni-potsdam.de

Citation:
Altdorff, D., Oswald, S. E., Zacharias, S., Zengerle, C., Dietrich, P., Mollenhauer, H., et al. (2023). Toward large-scale soil moisture monitoring using rail-based cosmic ray neutron sensing. *Water Resources Research*, *59*, e2022WR033514. https://doi.org/10.1029/2022WR033514

Received 23 AUG 2022
Accepted 9 FEB 2023

Abstract Cosmic ray neutron sensing (CRNS) has become a promising method for soil water content (SWC) monitoring. Stationary CRNS offers hectare-scale average SWC measurements at fixed locations maintenance-free and continuous in time, while car-borne CRNS roving can reveal spatial SWC patterns at medium scales, but only on certain survey days. The novel concept of a permanent mobile CRNS system on rails promises to combine the advantages of both methods, while its technical implementation, data processing and interpretation raised a new level of complexity. This study introduced a fully automatic CRNS rail-borne system as the first of its kind, installed within the locomotive of a cargo train. Data recorded from September 2021 to July 2022 along an ∼9 km railway segment were analyzed, as repeatedly used by the train, supported by local SWC measurements (soil samples and dielectric methods), car-borne and stationary CRNS. The results revealed consistent spatial SWC patterns and temporary variation along the track at a daily resolution. The observed variability was mostly related to surface features, seasonal dynamics and different responses of the railway segments to wetting and drying periods, while some variations were related to measurement uncertainties. The achieved medium scale of SWC mapping could support large scale hydrological modeling and detection of environmental risks, such as droughts and wildfires. Hence, rail-borne CRNS has the chance to become a central tool of continuous SWC monitoring for larger scales (≤10-km), with the additional benefit of providing root-zone soil moisture, potentially even in sub-daily resolution.

1. Introduction

Soil water content (SWC) is one of the crucial variables that govern key processes and conditions in the environment, such as atmospheric interaction, water balance, infiltration and percolation rates, groundwater recharge, and stream water fluxes. Consequently, information about SWC with adequate spatial and temporal resolution is required for a variety of scientific and practical applications such as hydrological investigations, crop production, forestry and wildfire risk assessment. While robust SWC information from field scales (<1 km) to medium scales (1–10 km) is difficult to obtain by traditional field methods (e.g., soil coring), proximal soil sensing techniques (PSS) (e.g., Rossel et al., 2011) offer a welcomed alternative to generate SWC data at these scales. The basic idea of PSS is to observe (relatively) easily measurable soil properties as a "proxy" for the desired variable. Electrical-based, hydrogeophysical techniques, such as electromagnetic induction and ground penetrating radar, have become particularly prominent for non-invasive SWC mapping (Altdorff et al., 2018; Huisman et al., 2003; Robinson et al., 2008). However, hydrogeophysical methods demand *in-person* field operation and its application is often accessibility restricted (temporal and spatial), which limits the information of the mapped areas to certain field days and predefined areas. Moreover, on ground hydrogeophysical methods do not (yet) reach the desired data resolution at the large scale (10–1,000 km), which is most relevant for hydrological modeling. In contrast, cosmic ray neutron sensing (CRNS) offers the possibility for continuous passive SWC data collection while the measured footprint of several hectares qualifies CRNS to bridge the information gap between classical hydrogeophysical approaches and most remote sensing products (Döpper et al., 2022; Heistermann et al., 2021; Meyer et al., 2022; Zreda et al., 2008) or hydrological modeling (Patil et al., 2021).

Numerous studies have demonstrated the successful application of CRNS for SWC monitoring at different test sites and under various conditions (Fersch et al., 2020; Heidbuchel et al., 2016; Heistermann et al., 2022; Jagdhuber et al., 2018) after its initial introduction by Zreda et al. (2008), and its technical implementation by Desilets

et al. (2010) and Zreda et al. (2012). Stationary sensors offer the advantage of covering areas over long periods in high temporal resolution, allowing for the observation of seasonal and temporal hydrological responses (e.g., Bogena et al., 2022; Schattan et al., 2017). Yet, due to the fixed position of the sensor, the information provided by stationary CRNS sensors remains restricted to the predefined footprint area. Various studies hence suggested a combination of several CRNS sensors to networks, either on a national scale as distant locations in the landscape (Avery et al., 2016; Bogena et al., 2022; Cooper et al., 2021; Evans et al., 2016; Zreda et al., 2012) or arranged adjacent to each other as a cluster to extend the mapped area and offering information about spatial SWC variability within its cumulative footprint (Fersch et al., 2020; Heistermann et al., 2022). Neutron simulation software, allows to predict the amount of neutron counts for given site conditions and sensor charateritics and has helped to interpret the understanding of soil-neutron-sensor interactions in the last years (e.g., Andreasen et al., 2016; Köhli et al., 2015, 2018; Zreda et al., 2008). Novel three-dimensional simulations, for example, performed by URANOS (Köhli et al., 2023) further support the disentangling of the signal integral and helped to define a practical footprint definition and that considers the relative contribution of remote or nearby areas (e.g., Schrön et al., 2023). While these advances have increased the understanding of the signal origin and allow for more precise interpretations, the mapped area of stationary CRNS remains restricted to its static footprint.

Car-borne CRNS roving, on the other hand, offers the possibility for SWC mapping of larger areas using portable, highly sensitive CRNS systems, transported in a manned vehicle that drives either on existing pathways or off-road. The idea of CRNS roving was first proposed and tested by Desilets et al. (2010) and further developed by Chrisman and Zreda (2013). Since then, the performance of car-borne CRNS systems has drastically improved and various studies demonstrated its successful application for expanding the investigated area and/or increasing the spatial resolution (Fersch et al., 2018; Franz et al., 2015; McJannet et al., 2017; Schrön, Rosolem, et al., 2018). Car-borne CRNS allows for quick and adaptive applications in areas of interest. Recent CRNS developments, such as increasing sensor capacities and the design of less expensive devices (Flynn et al., 2021; Weimar et al., 2020), approaches to exclude undesired vegetation and road effects (Baatz et al., 2015; Fersch et al., 2018; Jakobi et al., 2020; Schrön, Rosolem, et al., 2018), and efforts to additionally narrow the footprint area (Badiee et al., 2021; Jakobi et al., 2021) have made the use of car-borne CRNS roving even more attractive. Still, large detectors and precise supporting data for soil and vegetation properties are required to achieve high signal-to-noise ratios at the desired spatial resolution. Car-borne CRNS roving is further dependent on the traffic conditions, while the number of nearby cars and the change of lanes on multi-lane roads might have the potential to influence the measurement. Finally, car-borne CRNS demands active in-person operation and is—similar to most hydrogeophysical methods—campaign-based, and, as such a "snap shot" of information only, providing spatial SWC pattern rather than monitoring the spatio-temporal variation.

As an alternative, regular collection of CRNS data based on existing transport infrastructure, such as public or cargo trains as recently suggested by Schrön et al. (2021), promises to combine the advantages of both, stationary (providing continuity in time), and mobile CRNS techniques (providing continuity in space for medium to large scales) while it allows for repeatable measurements without supervision and fewer traffic-related restrictions. Schrön et al. (2021), showed the general feasibility of rail-borne CRNS (Rail-CRNS) through theoretical and experimental analyses. The authors demonstrated with a first order conceptual analysis that the sensitivity to the measured SWC is almost unperturbed by train material and only little by cargo or the presence of passengers in adjacent wagons. The results further showed that Rail-CRNS was able to delineate spatial variation of SWC and snow cover along the railway.

While Rail-CRNS has the potential to become a novel approach for continuous and transregional SWC data collection under minimal infrastructural investments, its technical implementation, data processing, and interpretation raises new challenges. In this study, we are pursuing this idea and present the next step by introducing a tailored Rail-CRNS detector system installed in a common electrical locomotive of a cargo train as the first and novel of its kind. We assessed the overall performance of the system by several independent local SWC measurements, car-borne CRNS, a local CRNS station, and weather data. In particular, we were interested to see whether Rail-CRNS would allow for capturing the spatial variability of SWC as expected due to differences in vegetation and land cover features within the region (~360 ha) and whether Rail-CRNS could resolve the temporal response of SWC to hydrological processes at daily and seasonal scales. By testing the technical and analytical requirements of an automatic Rail-CRNS approach, this study aimed at pioneering SWC monitoring at the large scale with a daily temporal resolution.

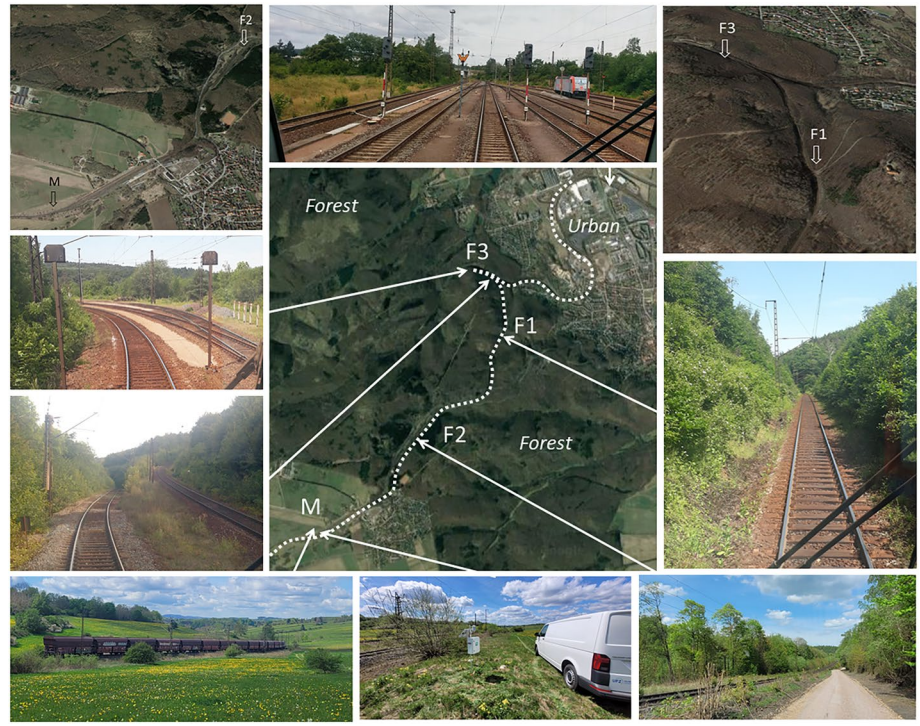

Figure 1. Photographs of the study region and parts of the railway track. The pictures reveal the complex environments of the urban area (top middle, close to the station at Blankenburg), the shunting area near F3 (left), the dense forest valleys near F1 (right), the open forest area near F2 (bottom right), and the grassland meadow M (bottom left) including typical railway wagons, the stationary Cosmic ray neutron sensing (CRNS) probe, and the mobile CRNS rover. Satellite photography: Google Maps.

2. Methods

2.1. Test Site

The study took place along a ∼9 km long railway section between the town of Blankenburg (51°79′N, 10°95′E) and the town of Rübeland (51°75′N, 10°84′E), in the Harz Mountains, Germany. The deployed cargo train belonged to a German railroad company (HVLE, Havelländische Eisenbahn Gesellschaft, http://www.hvle.de) and was running on a railway track owned by a mining company (Felswerke GmbH, http://www.fels.de) to load crushed limestone from quarries around the Rübeland station and unload its cargo at the bottom station at Blankenburg. The railway crosses an elevation of around 250 m (212–477 m a.s.l., slope up to 41%) and three main land cover areas (CLC (CORINE Land Cover), 2018): (a) urban; (b) forest and semi-natural areas; and (c) agricultural areas, dominated by meadows and hedges (Figures 1 and 2, and Figure A1).

The forest is a beech forest with alder and ash trees along the creeks while hay meadow and pasture dominated the agricultural areas (Stadt Blankenburg, 2021). Predominate soil types along the railway are different types of cambisol, consisting of loamy silts from glacial drift (LGB (Landesamt für Geologie und Bergwesen), 2021). The average annual temperature and precipitation (1999–2019) at Blankenburg are 9.1°C and 760 mm, respectively; the warmest month is July (18.3°C) and the coldest is January (0.2°C) (https://en.climate-data.org). The considered railway section is mostly single track with a few multitracked segments (near stations and shunting areas) covering less than 10% of the route. Toward the hill station at Rübeland, the train passes a tunnel and a bridge as well as several stretches, partially carved into the land surface. The train moved with an operational speed of approximately 10–30 km hr^{-1} for most of the railway parts. Regularly stops (>10 min) outside the stations occurred only at the shunting area (Figures 1 and 2, F3).

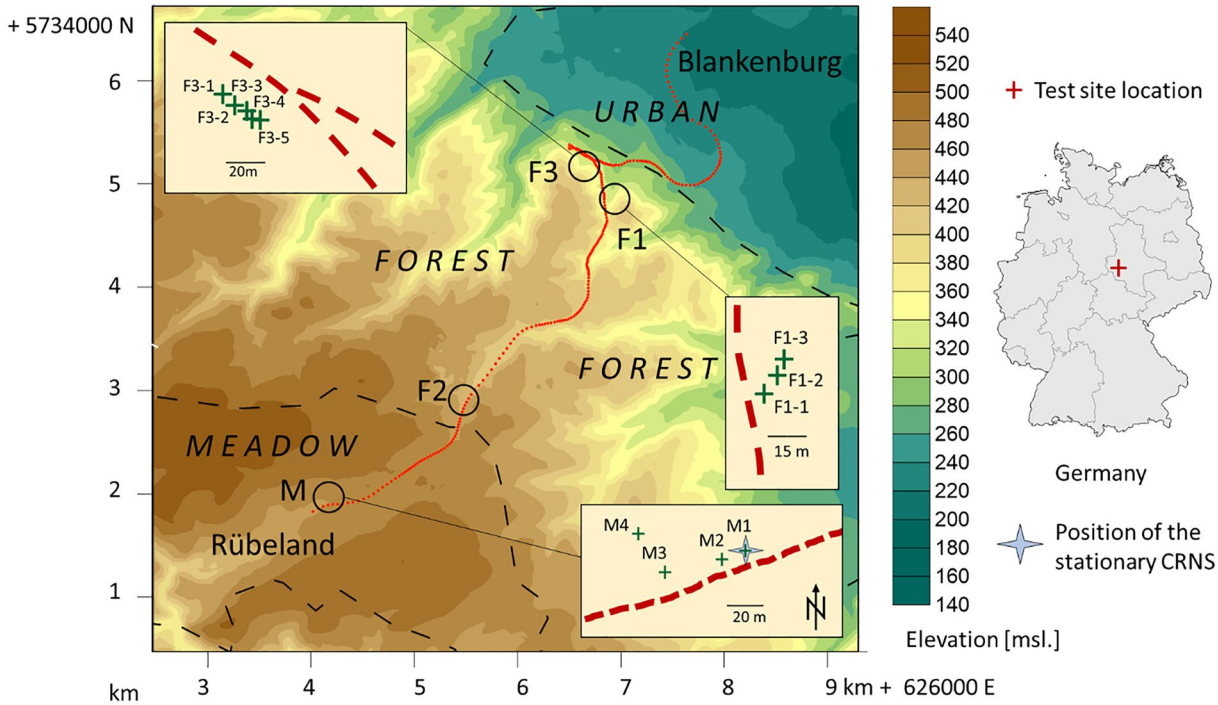

Figure 2. Investigation area in the Harz Mountains, Northern Germany, and monitoring infrastructure: Railway track with Rail-CRNS positions of the reference grid (red dots), sample locations (circles), location of the local wireless soil moisture sensor networks (WSN) including the positions of individual WSN nodes (green crosses), position of the stationary Cosmic ray neutron sensing sensor (at M1) and their location relative to the railway track (red dashed line). Land cover is indicated in three coarse categories (dashed black lines), that is urban, forest and agricultural areas (meadow). The local rain sensor is placed ~4 km west of M (elevation data from LGB, land use units based on CLC).

2.2. Instrumentation and Field Setup

2.2.1. Working Principle of CRNS

CRNS is based on the inverse relationship of naturally occurring secondary neutrons and the SWC of the surrounding area. CRNS measure neutrons within the epithermal energy range (>0.2 eV to 1 MeV) which is particularly water-sensitive due to the hydrogen in water which decelerates the neutrons during each collision (Desilets et al., 2010; Zreda et al., 2008). This causes dryer soils to have a higher probability of producing epithermal neutrons, while wetter soils have a higher probability of thermalizing and absorbing neutrons, which in turn lowers the detectable quantity above the surface. Neutrons can travel hundreds of meters from their location of reflection to the detector (Köhli et al., 2015), while the gross of the detected counts originates from albedo fluxes (scattering back within the upper soil) rather than direct soil emission (Köhli et al., 2021). While 40% of detected neutrons originate from an area of 20–40 m around the sensor, depending on the humidity of the environment, 60% of detected neutrons originate from more distant areas within the sensor footprint, which can be 100–200 m in radius, depending on the wetness of the area. Its effect on the recorded signal thereby decreases non-linearly with distance and depth to the sensor (Desilets & Zreda, 2013; Köhli et al., 2015; Schrön et al., 2017). Wet soil conditions and high air humidity also lower the CRNS footprint (Köhli et al., 2015; Schrön et al., 2017). The CRNS footprint is defined as the area from where 86% of the detected neutrons have interacted with the soil (Desilets & Zreda, 2013; Köhli et al., 2015).

2.2.2. Rail-CRNS

Following the pioneering work of Schrön et al. (2021), we searched for potential railway partners, who could provide a suitable infrastructure to allow for a continuous operation of a CRNS detector on a cargo train. This study used a Bombardier BR 185 locomotive (Bombardier Inc., Canada) from our cooperative partner HVLE; an electric locomotive, frequently used in Germany and Europe, thus providing the chance to extend the Rail-CRNS recording approach towards a wider context after its initial development. The geometry of the locomotive was measured for potential assembling spots and the dimensions and other specifications were forwarded

Figure 3. Assembling of the Rail-CRNS sensor into the BR 185 locomotive; here lifting the main unit (left) and the BR 185 while passing the meadow area (right).

to the manufacturer of CRNS equipment, Quaesta Instruments, USA (https://www.quaestainstruments.com), for a unique, custom-tailored solution. In close cooperation with Quaesta Instruments, a fully automatic and energy-efficient CRNS unit was developed, that allows for robust and high-performing neutron (N) recording and remote "on the fly" data control. The developed design guaranteed moreover absolute freedom from interferences to the surrounding electronics of the locomotive and railroad control systems. The final version used a pairwise Helium-3 gas tube system, which is a relatively expensive CRNS gas but it is inexplosive and hence met the railway safety requirements. Helium-3 tubes are further smaller in size compared to other options, allowing for space-efficient customization within the already instrumented locomotion. Additionally, He-3 is a nontoxic gas which could be used in public areas. The system allows for extending up to four tubes, which would increase the neutron counting performance by ∼1.5 times. The tubes were surrounded by a Boronated thermal neutron moderator (Shieldwerx, USA) and could reach up to 20,000 counts hr^{-1} (cph) which is about 333 counts per minute (Quaesta Instruments, USA). Undesired contributions from the subjacent railway track were expected, similar to the so-called "road effect" in car-borne CRNS roving (Schrön, Rosolem, et al., 2018). Hence, the detector was additionally shielded at the bottom by 15 cm thick polyethylene plates to reduce neutrons entering directly from below (Schrön et al., 2021). The system further featured georeferenced data recording, external (and internal) air humidity, air pressure and temperature sensing as well as data transmission by telemetry, as these variables are

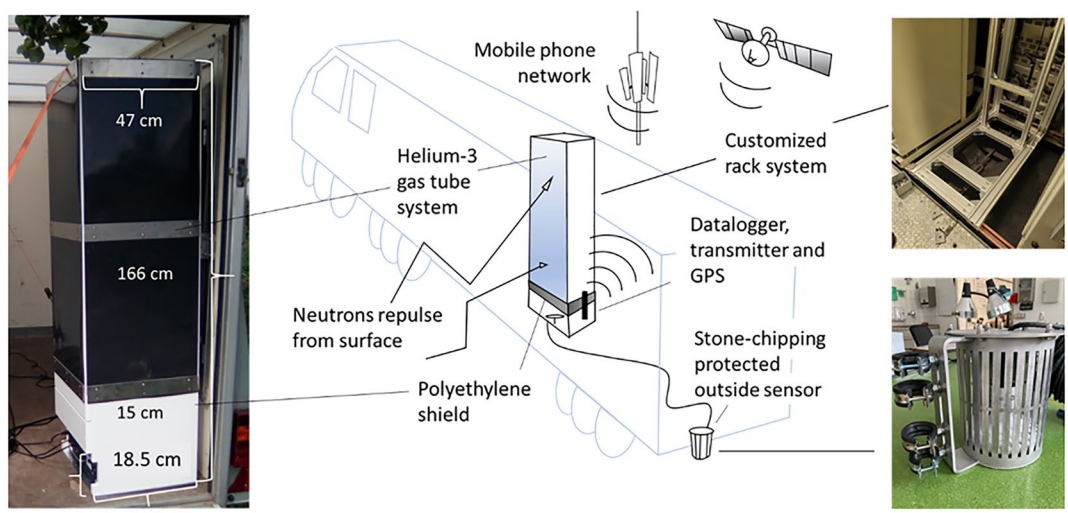

Figure 4. Schematic sketch of the Rail-CRNS system components and their relative placement within the locomotive.

required for the correction of incident neutrons and for accurate SWC estimation (see Section 2.3.2). The main part had the dimensions of 47 × 47 × 166 cm and a total weight of 140 kg (Figures 3 and 4).

According to international regulations, installation for railway vehicles must meet specific security and safety guidelines. Given the dimensions and weight of the CRNS system, the installation and mounting needed particular consideration. Here we took advantage of the inherent Bombardier busbar rack system by building a similar rack unit in consultation with the operating company HVLE. While neutron counting, GPS and telemetric functions were not expected to be influenced by its placement within the BR 185, the meteorological sensor needed to be fixed outside. We placed this sensor at a safe position underneath the locomotive and fixed it with a pipe clamp. Cables were run through an existing cable channel to the main system. The external sensor was further surrounded by a steel case (20 × 15 cm ⌀) to protect it from stone chipping (Figure 4).

All assembly and installation steps were completed in ~4 hours on 6 September 2021 at the Blankenburg cargo station. The system was connected to the electric power supply of the BR 185 and additionally supported by an internal 12 V battery. During the test phase, the energy consumption was very low (2 W under the normal running condition with occasional spikes up to 4 and 10 W during data transmission). Data sets were transmitted to an FTP (File Transfer Protocol) server by telemetry every 2 hr, allowing for real time data control and displaying. Due to the temporal aggregation of neutron counts inherent for all CRNS systems, roving CRNS always averages its information along its path while recording. Therefore, the aggregation time needs to be seen as a tradeoff between spatial resolution and signal-to-noise (Jakobi et al., 2021; Schrön et al., 2021) while higher neutron count sensitivities allow for higher spatial resolution. Our Rail-CRNS system provides a neutron count sensitivity between common stationary CRNS detectors and the few car-borne CRNS roving systems currently available. The data recording period was set to a small value of 5 s to enable flexibility in time aggregation during further data processing. Finally, the sensor was set to hibernate after 3 hr of running on internal battery and to restart when the external power supply becoming available again, as the locomotive eventually stops or starts, usually at night and in the morning. Each movement of the train was thus accompanied by Rail-CRNS measurements, but battery power and memory were spared when the locomotive was idle.

2.2.3. CRNS Rover (Car-Borne)

A mobile car-borne CRNS rover system manufactured by StyX Neutronica GmbH, Dossenheim, Germany (Heistermann et al., 2022; Weimar et al., 2020) was also deployed for comparison with Rail-CRNS observations. It contained eight modules with four detector tubes each, based on solid boron-10 proportional counters filled with $ArCO_2$. The recording time was set to 10 s to allow for high spatial resolution of the track path. The car-borne survey was carried out during the Rail-CRNS measurements at the main calibration locations (M, F1, F2, see the Section 2.2.4) and on the roads in between, favoring parallel road tracks close to the railway track if possible. Like Rail-CRNS, Car-CRNS roving faces the challenge of specifying spatial correction parameters and road conditions. Soil and land use correction was thus based on the same data sources as for the Rail-CRNS data processing to maximize comparability. The universal N_0 of the rover has been calibrated on the soil sampling points at the main calibration locations. Due to the short record periods, the single data points from the rover showed high variations, which is a typical challenge in mobile CRNS roving (e.g., Jakobi et al., 2021). We therefore, applied a similar spatial aggregation approach as proposed for the Rail-CRNS data (interpolating the raw data and re-gridding them to predefined master grid coordinates). Initial results showed that a block Kriging interpolation (including variogram analysis) resulted in more realistic SWC features than the nearest neighbor interpolation and are shown in the result section. We displayed the car-borne positions within a distance of <1,000 m to the railway.

2.2.4. In Situ SWC Measurement

Depth specific soil samples were collected at different parts along the railway, where the SWC was expected to vary the most based on preliminary Rail-CRNS surveys and data from M, F1, and F2 (n = 2–4 per site and day, total = 12). The samples were taken by a Purkhauer split tube system from 0—30 cm in 5 cm depth increments, while at some positions only 20 cm could be reached due to the stony soil. Samples were laboratory analyzed: (a) dried at 105°C for 24hr, (b) heated at 400°C for 16hr and (c) burned at 1000°C for 13hr, weighed at each step to obtain (a) the gravimetric SWC, (b) the soil organic content (SOC) and (c) the lattice water (LW), respectively (e.g., Altdorff et al., 2017; Fersch et al., 2020). Due to a technical issue with the muffle furnace, no ignition loss data were available for F2. We here assumed a combined SWC of 0.05 (0.03 SOC + 0.02 LW) as these

values were supported by similar values of our own test site and by the available soil maps (see also Figure A2). The vertical footprint of approximately 25–30 cm as observed by the initial Rail-CRNS analysis was used to compute a depth weighted average of the soil samples with weights of 75%, 15%, and 10% representing 0–10 cm, 10–20 cm, and 20–30 cm, respectively, to match the Rail-CRNS signal portions (Schrön et al., 2017). In the following analysis, we used gravimetric SWC because of the uncertainty in the bulk density data.

To assess the temporal performance of the Rail-CRNS, the study was further supported by small flexible wireless soil moisture sensor networks (WSN) (Fersch et al., 2020; Schrön, Zacharias, et al., 2018). The WSNs were initially installed at two railway stretches where the SWC was expected to be relatively low (M—meadow), and high (F3—forest). Further investigations however, showed that the wettest part was several hundred meters south. Hence, we added an extra WSN (sampling area F1) to cover the full range of SWC values (Figure 2). The WSNs contained 3–4 dielectric recording stations, set at 7–30 m distance to the railway track. Each station consists of six standard SMT100 probes (Truebner GmbH, Neustadt, Germany), buried pairwise at 10, 20 and 30 cm depth for automatically collecting dielectric permittivity (every 30 min). Conversion into SWC was done by using Topp's mixture equation (Topp et al., 1980), further conversion from volumetric into gravimetric SWC by using the bulk density from the soil samples. WSN station values were averaged for daily values and by location. During the initial analysis, we experienced unrealistically low SWC values from all recording stations at F1 compared to gravimetric SWC sampling (up to 30% lower); either by missing physical contact from the electrodes within the very stony soil or by the high amount of root penetration. Thus, we excluded the F1 WSN data from further analysis but kept studying this particular wet location for invasive soil sampling and Rail-CRNS analysis. The remaining two WSNs (F3 and M) recorded consistent data from 19 November 2021 onwards.

2.2.5. Stationary CRNS Measurement

We also employed a commercially available stationary CRNS sensor from May 2022 onwards to compare these results with the SWC from the Rail-CRNS system. The stationary CRNS sensor was a Finapp-5 neutron, muon and gamma-ray detector based on ^{6}Li and scintillator technology (Finapp s.r.l., Italy; see also Stevanato et al., 2019; Gianessi et al., 2022). The sensor was installed at the meadow site M, close to one of the WSN nodes (cf. Figures 1 and 2), and provided average raw counting rates of 2635 cph during the study period. Calibration of the N_0 parameter has been performed by minimizing the residuals of the SWC product to the spatial average of soil samples ($n = 3$) and topsoil Frequency Domain Reflectometry (FDR) values ($n = 173$) using the distance- and depth-weighting approach suggested by Schrön et al. (2017). We processed the data from the stationary sensor using the Desilets equation ($N_0 = 4{,}913$ cph) and an aggregation time of 24 hr.

2.2.6. Precipitation Data

This study used two sources of precipitation data: (a) publicly available data from a nearby weather station (Wernigerode, distance to Blankenburg ∼13 km, distance to Rübeland ∼9 km) in daily resolution provided by the Deutscher Wetterdienst, DWD (via www.wetterkontor.de) and (b) independent data collected by an OTT Pluvio^{2}—weather station (Ott; Germany) installed 1 m above the surface at Rübeland, approximately 4 km distance west to the meadow site M; called “local” in the following. The OTT station provided gravimetric precipitation measurements every 10 min from 25 October 2021, onwards. The data were summarized to daily values (6 CET to 6 CET the next day) to match the DWD intervals.

2.3. Data Processing

2.3.1. Rail-CRNS Preprocessing

The recording of the Rail-CRNS sensor was triggered by an external power supply from train movements which lasted usually from 7 a.m. to 10 p.m. Each daily file contained therefore large amounts of data, irrelevant to the desired railway segments (due to longer stops at positions where loading or maneuvering work took place, predominately at railway stations). To filter the files for separate, directional uphill and downhill rides, the raw data were cropped to the desired railway segments by their coordinates while the stations' areas were left out. Next, the starting times for individual rides were defined by identifying all time steps, where the coordinates of the start and endpoints were reached. Leaps in time larger than 45 min were generally considered as a new take, while the newest time before the station coordinates were left was defined as the start of a new ride. To separate further shunting activities from actual rides, only connected time series were used if the middle point coordinate between the start and end point was passed. The separation resulted in 2–14 rides per day, usually 10 to 12 with an

average of about 300 CRNS recordings per ride. After separation of the individual rides, each ride was processed separately using the CRNS data processing tool Corny v0.6.9-10 (https://git.ufz.de/CRNS/cornish_pasdy), with a temporal moving average of 2 min (i.e., 24 time-leaped individual records each). This setting was found to be a reasonable compromise between spatial resolution and signal-to-noise. The number and GPS positions of the observations varied as a result of the variable velocity during the individual rides. To obtain data at identical locations for separate rides as requested for further analysis, each ride was resampled (nearest-neighbor interpolation, 120 m) and re-gridded to new locations using predefined master coordinates along the railway track (Surfer 8, Golden Software, USA), (see also Altdorff et al., 2018). For the definition of these master coordinates, we took advantage of the fact that the distribution from observation points from all rides had a similar characteristic in response to the railway conditions: the train always slowed down at certain stretches, for example, approaching curves and crossings, and accelerated at straight leveled parts, resulting in a spatial resolution of approximately 15–60 m in observation points, based on the 5 s recording intervals (Figure 2), while the distance weighted SWC value as plotted at this position originated (depending on the train speed) from an railway segment between approximately 300 to 1,000 m. Due to the load, the train was always slower during downhill rides. We hence derived the final master coordinates from a representative downhill ride that showed particularly high data density. Initial results revealed a particularly high variation in SWC from the majority of downhill rides, which was likely related to the occasional dust minimization management of the cargo, where the limestone was sprinkled with water on top, as well as to variations of the cargo loads itself. We hence decided to neglect all downhill rides and proceeded with the data of uphill rides only when the train wagons were empty. We then aggregated the data of all single rides to the daily average on the master grid to gain a high signal-to-noise ratio for high spatiotemporal resolution.

Moreover, we experienced a high amount of variability around the tunnel and bridge area close to the hill station in almost every data set, presumably due to diverse morphological and anthropogenic effects (e.g., shielding of incoming radiation, complex variability around man-made infrastructure). These areas were excluded from the final data set to be analyzed in this study which resulted in a total railway distance of ∼9 km and 289 grid observations points. This study investigated a total period of 312 days, from 7 September 2021 (first day on air) until 15 July 2022. Due to a mandatory monthly service of the locomotive and internal pausing (e.g., holidays, season break), for about 40 days no rides occurred.

2.3.2. Determining SWC From CRNS

To convert the neutron intensity to SWC, the raw neutron counting rates need to be corrected to the site-specific environmental conditions at the recording time such as the neutron incoming rate, altitude, barometric pressure and air humidity (Desilets et al., 2010; Zreda et al., 2008). Several equations were proposed to convert N counts into SWC based on empirical relation (Desilets et al., 2010; Köhli et al., 2015, 2021). In this study, we used the established calibration function and parameters suggested by Desilets et al. (2010) as described:

$$\theta_{\mathrm{grv}}(N) = \frac{a_0}{N/N_0 - a_1} - a_2 \tag{1}$$

Where θ_{grv} is the gravimetric water content, N is the neutron counting rate normalized to a reference atmospheric pressure and solar activity level, N_0 is the counting rate over dry soil under the same reference conditions, and a_i are fitting parameters (Desilets et al., 2010). The a_i parameters were defined by neutron physics simulations (resulting in = {0.0808; 0.372; 0.115}) while N_0 as a site- and sensor-specific calibration parameter, was determined once for the full data set by comparing the CRNS derived SWC versus the actual SWC in the field (e.g., Schrön, Zacharias, et al., 2018). While in theory, N_0 should represent a stable value over time, moderate temporal variations have been reported by various authors (e.g., Heidbüchel et al., 2016; Heistermann et al., 2021; Rasche al., 2021). Considering the large variety of site conditions along our 360 ha test site, the definition of site-specific individual N_0 was impracticable. Instead, we followed the idea of a universal N_0 which is applicable along all-time steps and areas. For the universal N_0 calibration, we used the weighted SWC from our soil samples, averaged by location (three different locations at three different time steps), and the corresponding averaged neutron counts from the local part of the railway track that could be assumed to be related to this particular area (Table 1, Figure A1). Using these four data pairs, we derived our universal N_0 by minimizing the total residuals (root mean square error, RMSE) between measured gravimetric SWC (soil samples) and predicted gravimetric SWC (Rail-CRNS) (Equation 1), using an automatic solver (30 non-linear iterations, Excel, Microsoft, USA) which resulted in a universal N_0 = 22,888 cph and a total RMSE of 0.0320 g/g.

Table 1
Calibration Values for the Determination of a Universal N_0 Parameter (Equation 1) by Minimizing the Difference Between Rail-CRNS Gravimetric Soil Water Content (SWC) and the Four Available In Situ Sampled SWC Measurements

Location	Date	θ Rail-CRNS	θ measured	Squared residual	Average count hr^{-1}	θ car-borne CRNS
M	September 30	0.288	0.315	0.0008	13,108	n.a
F1	November 19	0.409	0.420	0.0001	12,046	n.a.
M	May 12	0.319	0.264	0.0030	12,779	0.261
F2	May 12	0.295	0.311	0.0003	13,028	0.318
Universal	–	–	–	0.0320	–	–

Note. The resulting N_0 for the Rail-CRNS sensor was 22,888 cph.

As epithermal neutrons are sensitive to all kinds of hydrogen, the recorded signal contained also information from non-SWC sources, such as ponds, organic material, plant water, LW, and other dynamic contributors (Baatz et al., 2015; Schrön, Zacharias, et al., 2018). The neutron counts in this study were corrected by standard methods (Jakobi et al., 2021; Schrön, Zacharias, et al., 2018; Zreda et al., 2012) using minute-by-minute (Rail-CRSN) and hourly (stationary CRNS) incoming radiation from Jungfraujoch (http://www01.nmdb.eu/nest), and atmospheric conditions based on data from the internal weather sensors. We initially used raster data for clay content, SOC and bulk density provided by Soil Grids (https://soilgrids.org/) to obtain the volumetric water content from the Rail-CRNS (Franz et al., 2015; Greacen, 1981). After applying the particular correction, however, we experienced unrealistic artificial patterns within the Rail-CRNS results as a consequence of the course raster data and its sharp boundaries, this was particularly true for bulk density. These unlikely patterns occurred also when the raster data were smoothed equally to the Rail-CRNS data ($n = 24$). Information in adequate resolution was not available yet, consequently, we decided to work using gravimetric water content units [g/g] throughout this study and neglect soil map raster data. Information about land use was derived from the digital Corine map (https://land.copernicus.eu). Within the forest, we took a biomass correction factor of 1.1, which reduces the amount of neutron counts by 10%, based on an estimate of forest biomass to be about 10–15 kg/m^2 and the empirical relation for biomass correction according to Baatz et al. (2015). Biomass effects in the urban and meadow areas were neglected, as biomasses were assumed to be much lower. Roads affect the neutron counting of the roving sensor because they are mainly drier than the surrounding conditions and reflect more neutrons. To overcome this effect, a railway track correction was applied similar to the road correction proposed by Schrön, Rosolem, et al. (2018) to account for the dry bias of the track area. For our correction approach, we assumed a track bed width of 4 m and an effective track bed moisture of 0.12 g/g. The latter is twice the value used by Ižvolt et al. (2016), because we were able to reduce the track's dry bias already hardware-wise by the implementation of a polyethylene shield at the bottom diminishing the neutron counts from underneath, und thus a less extreme nominal value was needed for the correction procedure.

3. Results and Discussion

In this section, we will first examine an exemplary set of four consecutive days without recorded rainfall, plot the Rail-CRNS results and discuss the spatial pattern and its uncertainties. Then, we will compare the car-borne SWC data versus the Rail-CRNS values of a single field day. Finally, we will visualize the unique spatiotemporal data set over the whole study period and along the rail track, and we will assess the response of Rail-CRNS, stationary CRNS, WSN, and soil samples to the meteorological events with a special focus on the selected comparison sites (M, F1, F2, F3).

3.1. Soil Moisture Patterns

The pattern of the Rail-CRNS data shown in Figure 5 illustrates the typical SWC characteristics that appeared to be mostly stable over the whole monitoring period. Although CRNS based SWC is known to be affected by soil properties, such as clay content, soil organic carbon, and bulk density (Avery et al., 2016; Dong & Ochsner, 2018; Franz et al., 2015; Iwema et al., 2021), the revealed spatial SWC pattern showed no obvious concordance with the available soil maps (Figure A2). However, the observed pattern agreed with the expected land feature effects,

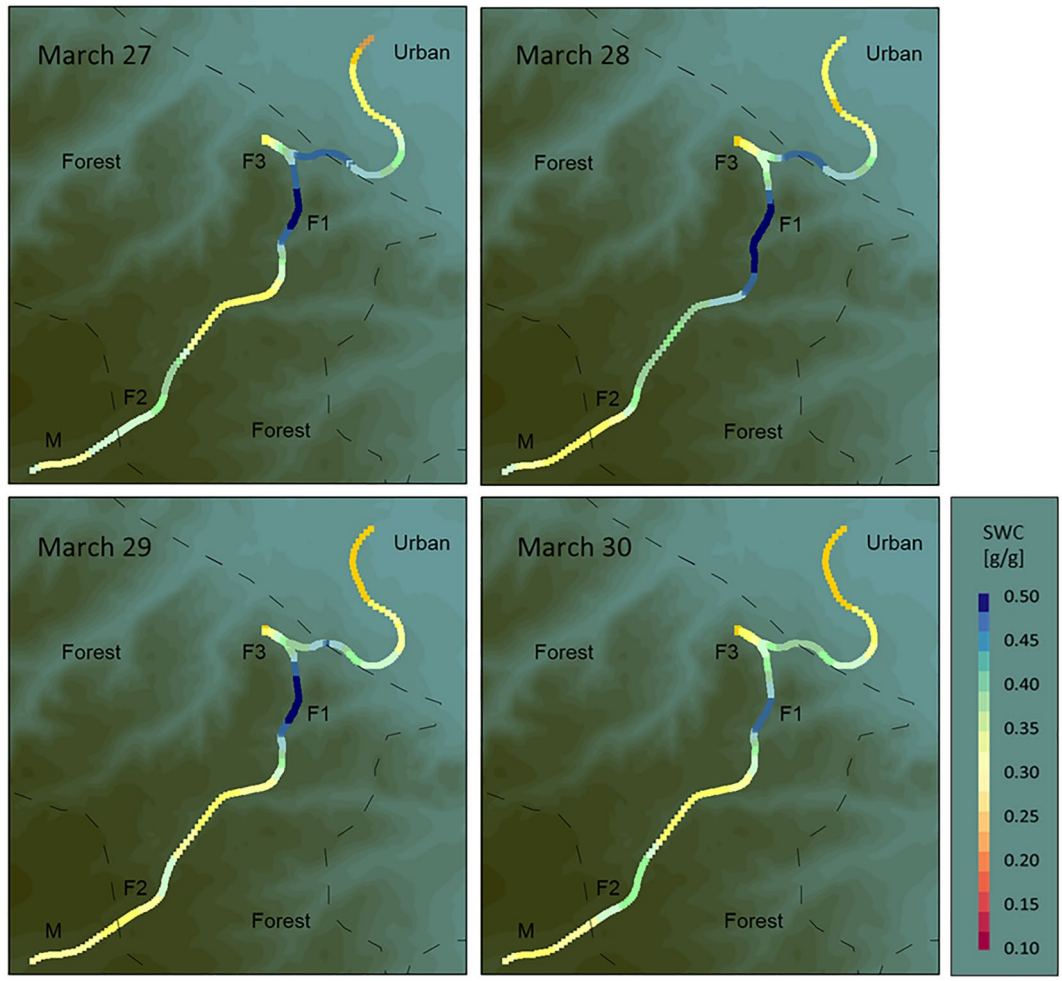

Figure 5. Rail-based soil water content results of four consecutive days out of a period without precipitation in March 2022, elevation contours (green-brown to green-gray) and an indication of land use units (dashed lines).

distinguished by its vegetation and anthropogenic features. The prominent dry segment measured near F3 is likely related to the train shunting area. At this part, the railway consists of multiple tracks, laterally extended and accompanied by a wide road (see also Figure 1). As per land use map (Figure A2), this area belonged to the forest and its neutron counts were corrected accordingly (see Section 2.2). However, the distance between the track bed and the first trees of the forest was much larger compared to other parts of the forest, which could have led to a lower influence of forest biomass on the detector and thus to a slight overcorrection at this site. In contrast, at the dense forest (F1), the trains run through a densely vegetated valley, where the railway track is close to the trees and partly dug into the landscape (compare also Figure 1). The measured high SWC can be interpreted as the result of the better exposure of the detector to the soil moisture in the surrounding area, higher water accumulation by overland flow, hilly terrain with a high number of puddles and thick litter layer, and less evapotranspiration due to less intense sunlight exposure. Moreover, the steep topography might have an influence on the neutrons counts too, an effect known as "topographic shielding." Its influence on stationary and roving CRNS is complex and still under discussion (Balco, 2014; Schattan et al., 2019). Although the presented study cannot fully rule out topographical shielding influence, the overall wet field conditions and the high SWC of the soil samples indicated that the gross of the lower neutron counts at F1 originated from higher soil moisture. The SWC decreased in the southern part as the forest becomes more open. After the railway passes the semi-open forest with smaller vegetation, the trees become denser again toward the boundary to the meadow (F2). In the meadow, the railway track consists again of a multi-tracked segment which can explain parts of the low SWC values (compare also Figure 1).

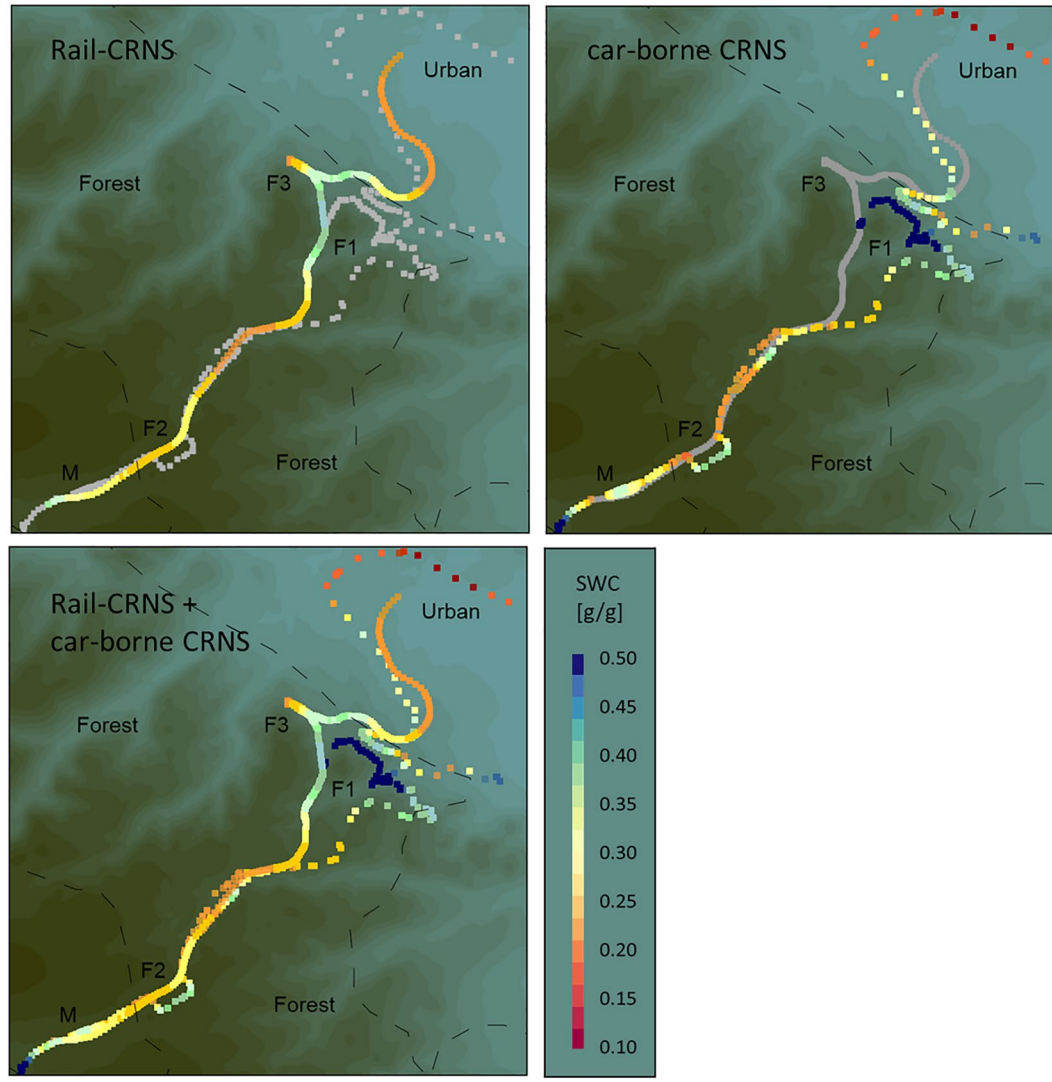

Figure 6. Soil water content results from the two Cosmic ray neutron sensing (CRNS) roving methods on 12 May 2022: (a) Rail-CRNS, (b) car-borne CRNS and (c) combined plot.

Although Figure 5 shows an extract from a period without precipitation recorded by the stations in the meadow, spatial and temporal variations in SWC are visible. For example, on March 28, the meadow (*M*) and the shunting area (F3) showed lower SWC than the day before which was qualitatively in alignment with a likely drying process. Similar to that observation, on March 30 the most prominent change is the drying of the F1 area. On the other hand, the central part of the railway and a part of the deep forest (south of F1) seemed to become wetter on March 28, without rainfall according to our weather data. Reasons for these so far unexplained increasing SWC recordings could be (a) local precipitation or fog in the forest that has not been recorded by the rain gauges placed in distance of a few kilometers, (b) unusual cargo load or wagon configuration which has not been reported, (c) atmospheric changes that may have locally influenced incoming neutrons, or (d) inherent statistical noise of the sensor signal.

3.2. Comparison of Rail-CRNS to Car-Borne CRNS

An exact evaluation of Rail-CRNS data points by the car-borne data points was not possible, since both systems recorded at different positions (the road did not overlap with the railway). Also, the differences in sensor shielding (see Section 2.2.2) and corresponding different sensitivities to near-field influences limited their direct comparsion (Schrön et al., 2017). However, the large overlapping footprints from both systems allow for quantitative comparison. A comparison of the two CRNS roving systems is shown in Figure 6 and confirmed the overall consistency

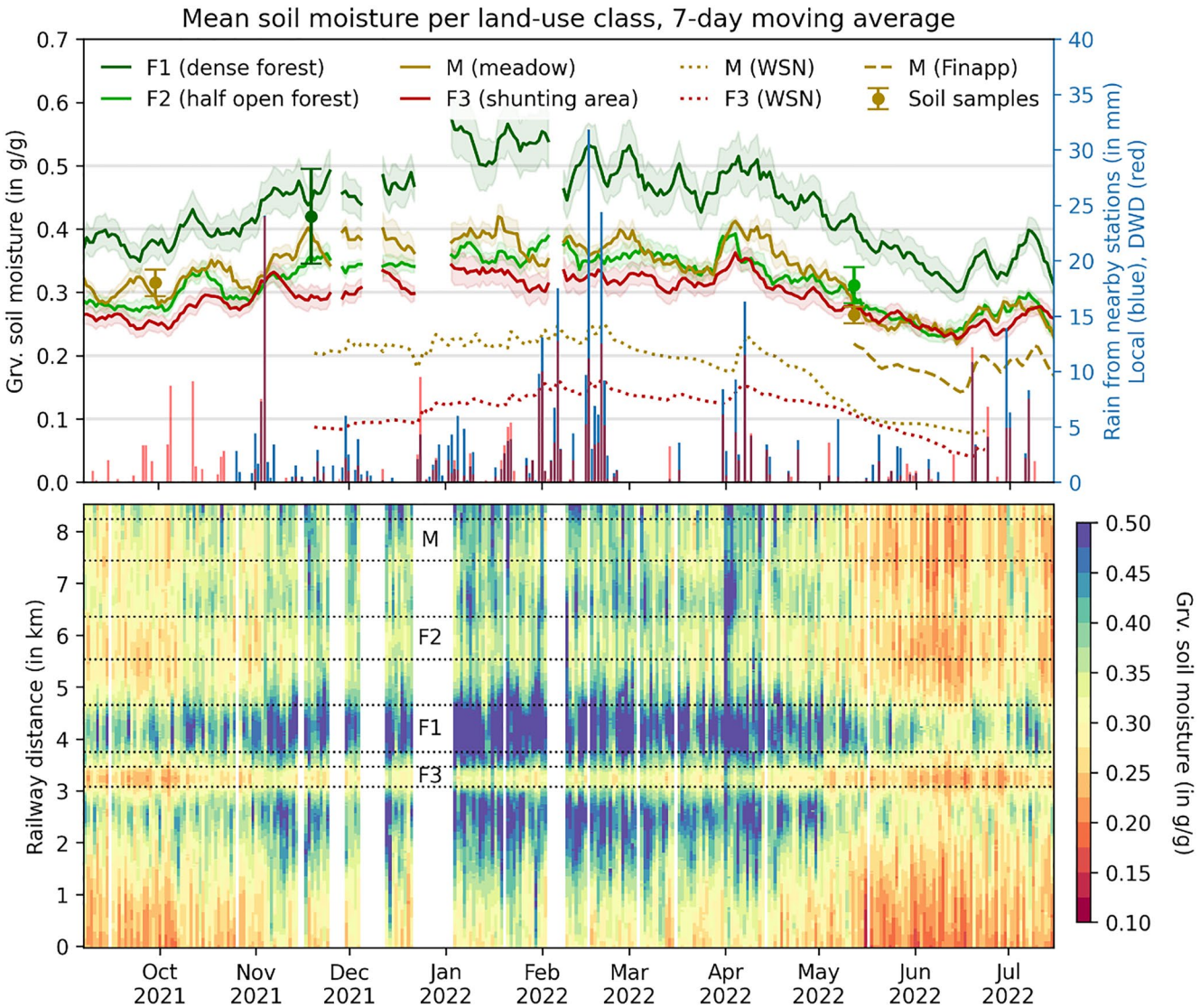

Figure 7. Results from the investigation period until mid-Jul 2022; the upper panel shows the precipitation data, measured several km from the railway track, the 7-day smoothed soil water content (SWC) time series by Rail-CRNS from the four sample areas, the SWC dynamics measured by the WSN, the SWC from the stationary Cosmic ray neutron sensing sensor (Finapp) and soil samples. The lower panel shows the daily SWC values by its grid points along the railway, plotted along the vertical axis as a 1D-profile and daily values plotted along the horizontal axis; starting at the urban area (0 km) toward the meadow (8 km) with indications of the local calibration areas F1, F2, F3, and M (dashed lines).

in the SWC pattern, as likely dominated by stable surface features. Both recordings display higher SWC within the dense forest around F1 and lower in the urban and meadow area. The diverging absolute SWC values, for example, higher SWC from around F2 as recorded by the car-borne system, was likely the result of the mentioned geolocational mismatch and varying road conditions. Moreover, here the car-borne CRNS was moving on forest track where the trees were located very close to the sensor (smaller road), while the Rail-CRNS data has been recorded in several meters distance to the edge of the forest due to the broader railway bed. The same is true for the highest SWC values (~0.50 g/g) around F1; here the car rover ran on a unpaved forestry track surrounded by dense trees (Figure 1).

3.3. Continuous Spatiotemporal Mapping

The complete response of the mapped area to precipitation, drying periods, and to the seasonal hydrological cycle is presented in Figure 7. In the top panel, the SWC timelines from the selected areas shows a consistent ranking: The denser forest F1 reached by far the highest SWC, the meadow and F2 followed, while the shunting area at F3

was always the driest part. This consistency over the full period substantiated the assumption of stable individual area features (such as track beds or morphology), which predominantly shaped the spatial SWC pattern. The magnitude of the gravimetric soil moisture pattern is stronger than what could be expected from typical variations of soil properties, such as clay content, LW, or bulk density (order of few percent).

In addition to the spatial SWC pattern, temporal variation can be observed by seasonal variations (wetter in winter, dryer in spring and summer), and by its response to single precipitation events. Further, Rail-CRNS and WSN lines expressed similar characteristics in their response to rainfall and drying events, particularly noticeable for the rise and fall in April and May. Both methods displayed the shunting area as particularly dry. The Rail-CRNS values are higher and more scattered than the corresponding lines from the WSN, particularly F1, although a 7-day moving average was applied on the daily values. We explained these alterations by methodological differences (CRNS vs. FDR SWC measurement). The high variation of measurements in F1, for instance, was caused by lower neutron counts, which naturally correspond to higher noise levels. It seems further, that the Rail-CRNS reacts partly more sensitive to rain events than the WSN (see, e.g., the response to the rain in mid-May). The uppermost WSN sensors were buried at 10 cm depth, to guarantee the minimum distance to the surface of 7 cm as required for accurate recordings (Truebner GmbH, Neustadt, Germany). Although the signal from the upper WSN sensors theoretically comprises an integral of ∼3.5–16.5 cm, they were apparently not sensitive enough to record the highly variable moisture dynamics of the upper soil horizons, at the surface, or intercepted on leaves and the litter layer. Those important hydrological compartments were only visible by the Rail-CRNS (Figure A4). The WSN sensors also showed much lower values compared to the data from the soil sampling campaigns, indicating that their spatial representativeness for the whole area is low (WSN—several point measurements, Rail-CRNS—integral over several hectares, see also Figure A3). This explanation was supported by the fact that the SWC from the stationary CRNS sensor at the meadow site (*M*) recorded higher SWC values and its temporary variation in response to rain events was much more in alignment to the Rail-CRNS at M (particularly visible in late June to mid-July) due to a greater overlapping in footprints (see also Figure A4). The still existing differences between the Rail-CRNS and the station can be explained (a) by differences in calibration approaches– (soil samples for the Rail-CRNS, additional FDR samples for the CRNS station, see Sections 2.2.5 and 2.3.2) (b) by differences in aggregation time—the Rail-CRNS data were aggregated over a few minutes per day (as the train passed along the meadow), while the station aggregated over 24hr per day, and (c) by differences in absolute footprint area—the Rail-CRNS data were recorded along a ∼600 m railway segment, hence containing more information from outside the stationary footprint radius than from inside. Nevertheless, the variances between daily and 7-day average values showed reasonably low deviations for the selected areas: M (3.3%), F1 (4.2%), F2 (2.9%), and F3 (2.1%). The total standard deviation along the full railway length (∼9 km) was 1.7%.

The spatio-temporal variation for daily SWC values, aggregated to the master grid points (lower panel Figure 7) visualizes the responses of the different railway segments to wetting and drying events. Particularly noticeable are the continuous dry shunting area (F3) and the wet dense forest (F1). Focusing on two periods in spring, the Figure demonstrates the robust performance of the sensor: the rewetting in early April, where the rain particularly increased the soil moisture of the upper part of the railway (from F1 upwards), and the drying drift from End of April onwards, a trend that even the occasional rainfall could not delay for very long. The plot shows further the beginning of the summer drought (see also UFZ, 2022; Zink et al., 2016); drier areas grow slowly from both sides into the forested areas. Wieser et al. (2022) observed similar forest resilience against drying periods using a limited number of snapshots, measured by the mobile CRNS rover, while the Rail-CRNS technology presented here allows for revealing these effects in a temporally continuous way. The data revealed further the rewetting process, particularly of the forest area, due to several summer rain events in late June and July, while the shunting area remained less affected. Based on these observations, the method may be able to support the regional assessment and modeling of forest resilience, long-term drought stress, and climate impact analysis.

3.4. Discussion and Outlook

Our study showed that constant and automatic long-term CRNS roving by trains is technically feasible and able to provide realistic results throughout the seasonal cycle of soil moisture variations. The current system provided reasonable spatial and temporal patterns at daily resolution. The comparison between the 7-day average and the daily averages however showed that further developments are needed to reduce the measurement uncertainty in Rail-CRNS roving. As the SWC patterns were sometimes inconsistent at the highest

temporal resolution (single rides), better technology to increase the signal-to-noise ratio, as well as further investigation toward potentially affecting temporal variables is also recommended. For example, the local natural background of incoming cosmic ray neutrons might have temporarily deviated from the data used as recorded at Jungfraujoch at > 600 km distance. Local incoming correction strategies with muon detectors have been recently suggested by Stevanato et al. (2022) and Gianessi et al. (2022), and might have the potential to correct existing deviations such as the unrealistic fluctuations observed during a day without precipitation) or shielded topographic terrain (e.g., F1). The prospects of higher sensor performance (i.e., increased counting rates), incorporation of additional land cover data (e.g., biomass), and more frequent calibration campaigns may increase the quality of the provided SWC product. Likewise, we would expect that detailed vegetation data in a sufficient resolution around the railway track could improve the biomass correction and hence the estimated SWC values. Reliable and highly resolved soil maps (~0.1 km scale) could further compensate for the effects of differences in soil properties on the estimated SWC variation. Studying the effect of railway architectures, such as multi-tracking, tunnels, bridges, etc. on signal stability is also needed to enlarge the current study area and to transfer the findings to other railway tracks. In addition, investigating the effects of topography on neutron counts and GPS accuracy, such as shielding by hill slopes, should be incorporated in future studies.

Further investigation needs to focus on variable train speed, shunting activities, as well as different types of cargo conditions, but also applicability at other sites and train environments as well as potential ship effects (e.g., Kouzes et al., 2008) from massive metal constructions. Finally, the validation of the overall Rail-CRNS results, for example, by a higher amount of soil samples and supporting CRNS data from additionally installed stations or car-borne roving campaigns, is the next step to adjusting the sensor calibration and quantifying the SWC results by its uncertainties (spatial and temporal). The suggested concept of Rail-CRNS should be tested on additional, longer routes of different complexity with varying ride frequencies. Considering the mentioned challenges, we would like to emphasize that the results presented here are just laying the foundation of a Rail-CRNS methodology while further improvement of signal stability during data recording and postprocessing (compare e.g., Franz et al., 2022) is clearly needed. By incorporating the recommended improvements however, we believe that Rail-CRNS has the potential to become a crucial technique for continuous SWC monitoring at medium scales, to produce data that could be useful for validation and improvement of numerical hydrological models. Satellite-supported rainfall data in higher spatial resolution (≤1 km) shall be beneficial to bring the observed small scale SWC variations and local precipitation events in (potential) alignment and could hence additionally help to interpret the signal variations.

The obtained SWC information could in turn also be used for identifying temporally stable subfield areas (e.g., Gibson & Franz, 2018), in our case for example F1 (constant wet) and F3 (constant dry). Moreover, the resulting SWC information from Rail-CRNS could be used as training data for model conditioning and extrapolation of the results into a larger area. The resulting SWC products might also be used directly as a baseline for adjusted land management strategies such as irrigation management (e.g., Finkenbiner et al., 2019).

4. Conclusion

The study presented the first rail-borne CRNS system for automatic and continuous SWC monitoring beyond the hectare scale. We proved that Rail-CRNS neutron detectors, mounted in a train locomotive or potentially in wagons, can run permanently and maintenance-free while providing highly resolved SWC data transmitted by telemetry. In this study, the system provided almost uninterrupted daily data from Sep 2021 to July 2022 along a 9 km railway track in the Central Harz mountains of Germany. As there is a strong demand from various user communities for SWC products at a kilometer scale, currently not sufficiently covered by satellite remote sensing products (e.g., Peng et al., 2021), the expanded footprint of the presented Rail-CRNS systems offers the chance to become a central tool of continuous SWC monitoring at large scales.

Our results have shown that Rail-CRNS can resolve spatial patterns as related to land cover (e.g., wetter forest, dryer meadow), seasonal dynamics (wet winter, dry summer) and individual responses of single railway segments to wetting and drying periods. For example, the spatiotemporal resolution revealed the different drying progress from different landscape units under starting drought stress in late spring. In the light of the intensified vulnerability of ecosystems to drought, floods, or forest fires, the method might be able to provide

important and near-real-time information that can be linked to hydrological modeling and remote sensing products. Still, some unexplained variations in the sensor signal need further investigation, especially when it comes to increased temporal resolution. Further theoretical studies on the influence of track bed, cargo, or topography, as well as practical studies on validation strategies and the inclusion of remote-sensing data, are needed to further improve the quality of the final SWC products.

Appendix A

A1. Site Description Along the Rail Track

The study region contained a mixture of various land features across three main land use types, starting in an urban area in the northern part, followed by a mountainous forest and a grassland meadow in the southern part as depicted in Figure 1 already via photographic material. In the middle ground in Figure 1, the figure shows multiple railway tracks in the urban area near the Blankenburg station, which leaded to particularly dry soil moisture values (shown for demonstration purposes only, since this area was excluded from the analysis). Also, the shunting area near F3 is a relatively open forest with two to three parallel railway tracks, which may be the reason why F3 appears to be consistently much dryer compared to the other forest areas. The dense forest valley near F1 exhibit sloped terrain with many spots compacting runoff water below the litter layers. These wet spots together with the short distance between railway track and forest trees lead to relatively high apparent SWC values. The open forest area near F2 runs through a sparse composition of trees and bushes and in between two dry roads, leading to relatively dry apparent soil moisture. The meadow site M consists of a large, hilly grassland right with a few bushes and trees next to a multi-track railway area. Figure A1 illustrates the land use parts and the main comparison sites along the track.

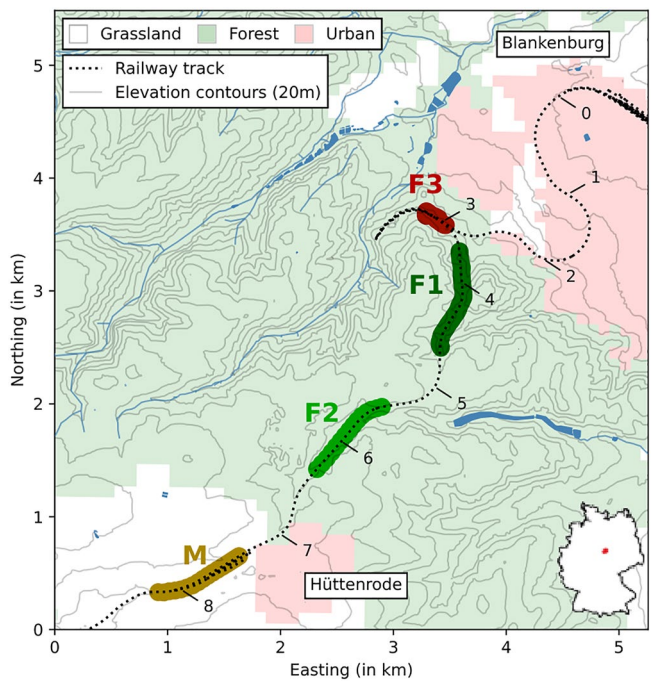

Figure A1. Simplified land use units based on CORINE (https://land.copernicus.eu/pan-european/corine-land-cover), railway tracks based on OpenStreetMap), distance along track numbered in whole kilometers starting from Blankenburg, and position of the selected areas F1, F2, F3, and M. Surface waters are shown in blue.

A2. Variation of Soil Properties

The variations of the soil properties, soil organic carbon content (SOC), clay content and bulk density are shown in Figure A2. None of the pattern as given by the maps stand in obvious relation to the revealed SWC variability

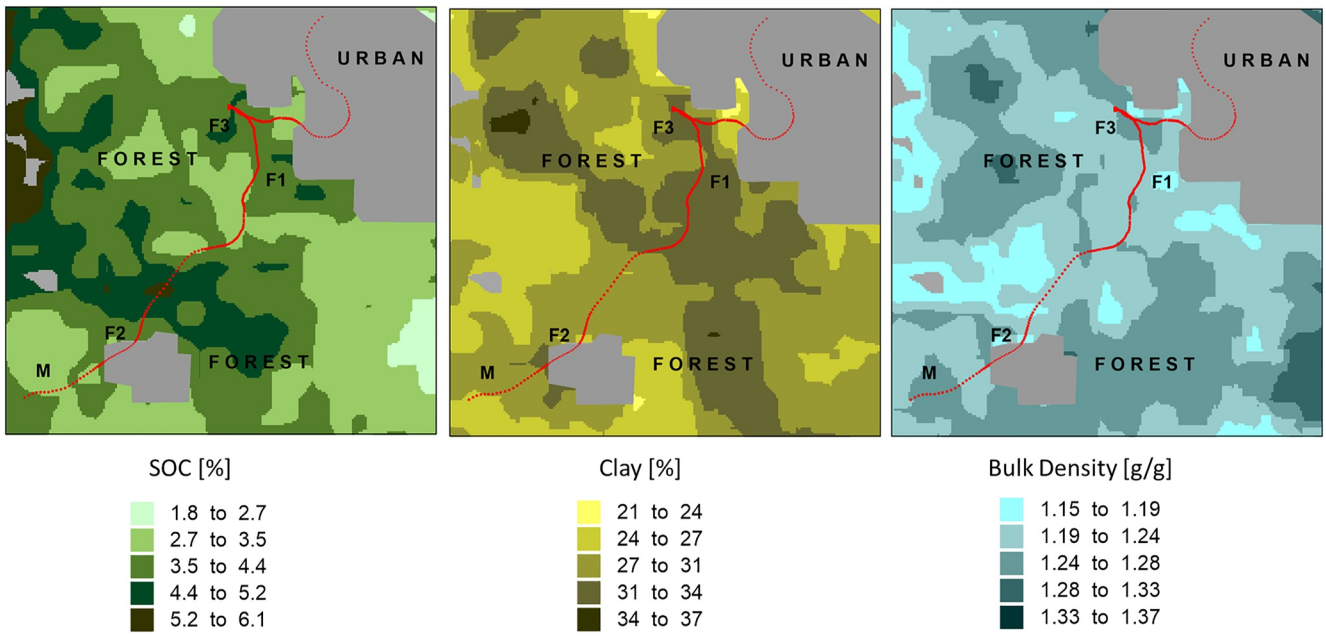

Figure A2. Soil maps for soil organic carbon content (soil organic content), clay content (clay) and bulk density based on raster data (https://soilgrids.org) (areas of no information and urban settlements are shown in gray).

(compare Figures 5 and 7). It is further noteworthy that the pattern from the soil properties are not in alignment with the current land use units (compare Figure A1).

A3. Comparison of Soil Moisture Measurements

Measurement campaigns at the comparison sites have been conducted in September 2021 and November 2021 with soil sampling, and in May 2022 with soil sampling and car-borne CRNS roving. Figure A3 shows a compar-

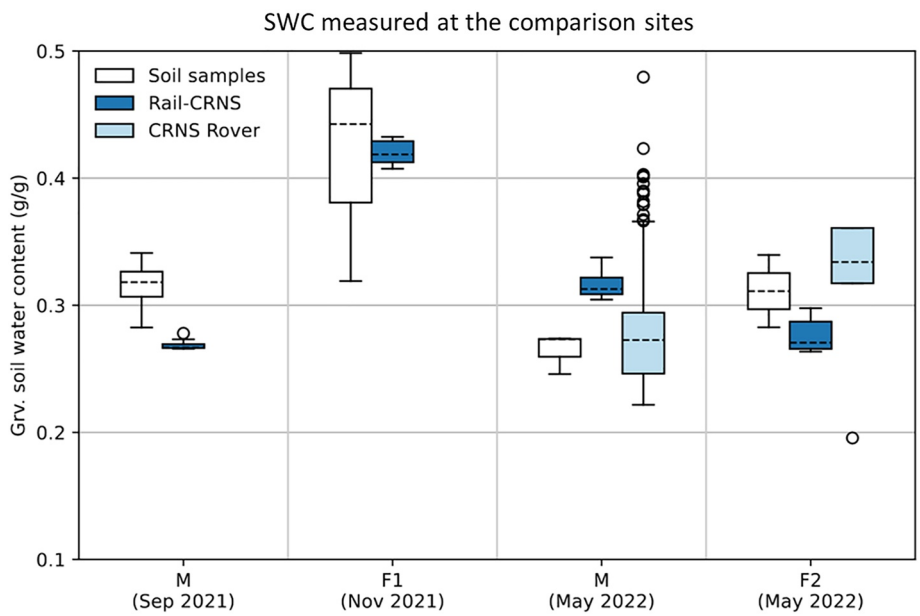

Figure A3. Box and whisker plot showing soil moisture measurements from soil sampling, Rail-CRNS in that area, and car-borne Cosmic ray neutron sensing roving near the railway track. Differences in the number of samples and soil water content values indicate different practicability of sampling measurement and different footprint representation.

ison of the various datasets in a boxplot. The values differ by the number of samples and by the representative footprint area. In particular, only a few soil samples have been taken near the railway track, while rover measurements are also limited by accessibility via roads, such that the area of influence between Rail-CRNS and car-borne CRNS is not necessarily identical.

A4. Comparison of SWC Results From Stationary CRNS Sensor

A stationary CRNS sensor (Finapp-5) was installed at the meadow site (*M*) on 12 May 2022 in approximately 10 m distance from the railway. Figure A4 shows a comparison of the Rail-CRNS data in the meadow section (*M*) with the continuously recording station. Although the absolute SWC showed an offset due to different calibration approaches, the temporal variations of both sensors were in good agreement, despite their differences in aggregation times and footprints, particularly visible by the wetting and drying from mid-June to mid-July. Comparing the response to individual rain events, it even occurred that the Rail-CRNS partly react more sensitively to smaller wetting events, for example, around May 25 and June 8.

A5. Wireless Soil Moisture Data

The wireless soil moisture sensors monitored the soil moisture state in two comparison sites, F3 and M, each equipped with three WSN nodes and two sensors per depth. The mean and standard deviation of the measurement signals for each depth are plotted in Figure A5. The data show that soil moisture variations are more dynamic in the upper soil layers, but also that the vertical soil moisture profiles in F3 and M are inverse. The forest site shows higher soil moisture in the upper layers, indicating low surface water evaporation (due to shadowing by leaves) and root-water uptake in deeper layers. In contrast, the meadow site M shows drier surface soil moisture, indicating higher surface water evaporation (no shadow effects) and low root-water uptake (due to shallower grassroots).

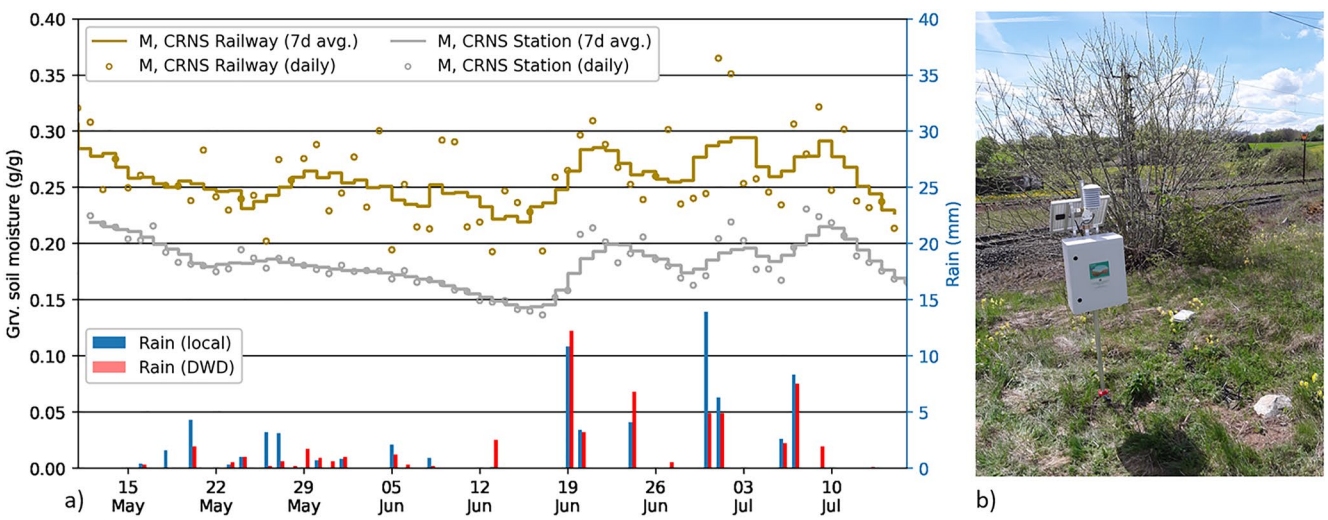

Figure A4. (a), Comparison of soil water content results from stationary Cosmic ray neutron sensing (CRNS) sensor (Finapp-5, as described in principle in e.g., Stevanato et al., 2019; Gianessi et al., 2022) and Rail-CRNS in response to various rain events (please note that the stationary sensor was calibrated site-specifically, while the Rail-CRNS was universally calibrated), (b) picture of the stationary CRNS sensor.

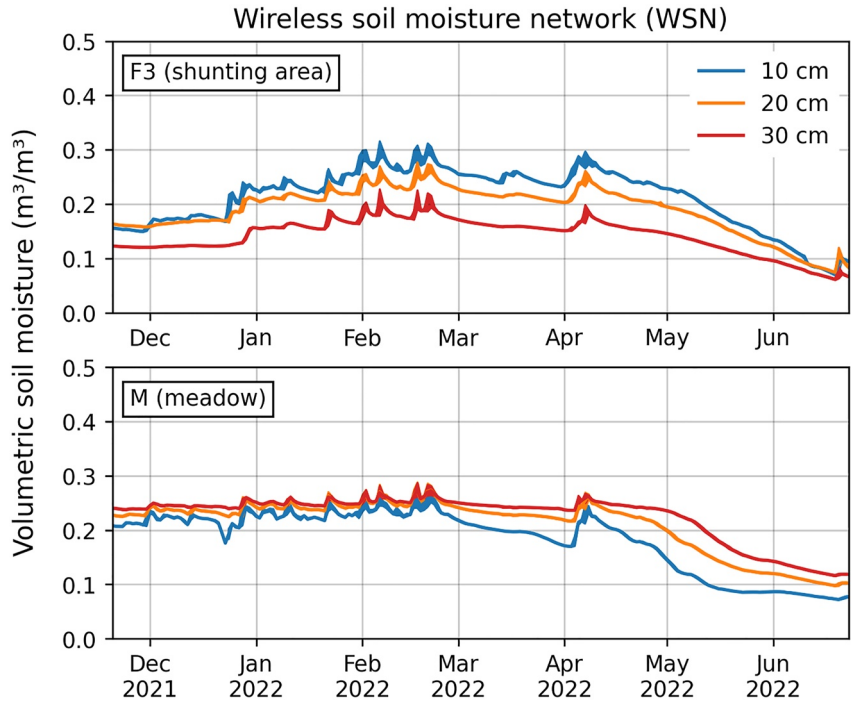

Figure A5. Time series of volumetric soil moisture as recorded by the WSN at F3 and M in the depths of 10, 20, and 30 cm. Line thickness indicates the standard deviation of available WSN sensors in the same depth.

Conflict of Interest

The authors declare no conflicts of interest relevant to this study.

Acknowledgments

The authors like to acknowledge the essential support of the UFZ—Helmholtz Centre for Environmental Research GmbH, Leipzig, Germany, for creating the research environment that allowed the study on Rail-CRNS. The authors like to thank further the crucial support from the Havelländische Eisenbahn Gesellschaft (HVLE), Wustermark, Germany, particularly from Dirk Brandenburg and Uwe Wullstein. Additional acknowledgments are going to Torsten Wöhler, Daniel Gehlmann and Andreas Harms from the Felswerke GmbH, Rübeland, and to Hardy Wichmann-Mimus, Leipzig, for consulting on railway operation practices. Special thanks belong to the technical development team Mathias Wilde, Julian Weber, Manuel Kositzke, Peter Portius (UFZ), to Gary Womack (Quaesta Instruments), and to the field technicians Christian Budach, Peter Biro (Uni Potsdam) and Manuel Kreck (UFZ). This work was supported by funding from the Deutsche Forschungsgemeinschaft (DFG) project 357874777 of the research unit FOR 2694 CosmicSense; the Helmholtz Association in the framework of MOSES (Modular Observation Solutions for Earth Systems); and by the Terrestrial Environmental Observatories in Germany (TERENO). Open Access funding enabled and organized by Projekt DEAL.

Data Availability Statement

The data used in this study are available under: https://dataverse.harvard.edu/dataset.xhtml?persistentId=doi:10.7910/DVN/O1MHKR. The Jungfraujoch neutron monitor data were kindly provided by the Cosmic Ray Group, Physikalisches Institut, University of Bern, Switzerland (http://www.nmdb.eu/).

References

Altdorff, D., Galagedara, L., Nadeem, M., Cheema, M., & Unc, A. (2018). Effect of agronomic treatments on the accuracy of soil moisture mapping by electromagnetic induction. *Catena*, *164*, 96–106. https://doi.org/10.1016/j.catena.2017.12.03

Altdorff, D., Galagedara, L., & Unc, A. (2017). Impact of projected land conversion on water balance of boreal soils in western Newfoundland. *Journal of Water and Climate Change*, *8*(4), 613–626. https://doi.org/10.2166/wcc.2017.016

Andreasen, M., Jensen, K. H., Zreda, M., Desilets, D., Bogena, H., & Looms, M. C. (2016). Modeling cosmic ray neutron field measurements. *Water Resources Research*, *52*(8), 6451–6471. https://doi.org/10.1002/2015WR018236

Avery, W. A., Finkenbiner, C., Franz, T. E., Wang, T., Nguy-Robertson, A. L., Suyker, A., et al. (2016). Incorporation of globally available datasets into the roving cosmic-ray neutron probe method for estimating field-scale soil water content. *Hydrology and Earth System Sciences*, *20*(9), 3859–3872. https://doi.org/10.5194/hess-20-3859-2016

Baatz, R., Bogena, H. R., Hendricks Franssen, H.-J., Huisman, J. A., Montzka, C., & Vereecken, H. (2015). An empirical vegetation correction for soil water content quantification using cosmic ray probes. *Water Resources Research*, *51*(4), 2030–2046. https://doi.org/10.1002/2014wr016443

Badiee, A., Wallbank, J. R., Fentanes, J. P., Trill, E., Scarlet, P., Zhu, Y., et al. (2021). Using additional moderator to control the footprint of a COSMOS rover for soil moisture measurement. *Water Resources Research*, *57*(6), e2020WR028478. https://doi.org/10.1029/2020wr028478

Balco, G. (2014). Simple computer code for estimating cosmic-ray shielding by oddly shaped objects. *Quaternary Geochronology*, *22*, 175-182. https://doi.org/10.1016/j.quageo.2013.12.002

Bogena, H. R., Schrön, M., Jakobi, J., Ney, P., Zacharias, S., Andreasen, M., et al. (2022). COSMOS-europe: A European network of cosmic-ray neutron soil moisture sensors. *Earth System Science Data*, *14*(3), 1125–1151. https://doi.org/10.5194/essd-14-1125-2022

Chrisman, B., & Zreda, M. (2013). Quantifying mesoscale soil moisture with the cosmic-ray rover. *Hydrology and Earth System Sciences*, *17*(12), 5097–5108. https://doi.org/10.5194/hess-17-5097-2013

Cooper, H. M., Bennett, E., Blake, J., Blyth, E., Boorman, D., Cooper, E., et al. (2021). COSMOS-UK: National soil moisture and hydrometeorology data for environmental science research. *Earth System Science Data*, *13*(4), 1737–1757. https://doi.org/10.5194/essd-13-1737-2021

CLC (CORINE Land Cover). (2018). Retrieved from https://land.copernicus.eu/pan-european/corine-land-cover

Desilets, D., & Zreda, M. (2013). Footprint diameter for a cosmic-ray soil moisture probe: Theory and Monte Carlo simulations. *Water Resources Research*, *49*(6), 3566–3575. https://doi.org/10.1002/wrcr.20187

Desilets, D., Zreda, M., & Ferré, T. P. A. (2010). Nature's neutron probe: Land surface hydrology at an elusive scale with cosmic rays. *Water Resources Research*, *46*(11), W11505. https://doi.org/10.1029/2009wr008726

Dong, J., & Ochsner, T. E. (2018). Soil texture often exerts a stronger influence than precipitation on mesoscale soil moisture patterns. *Water Resources Research*, *54*(3), 2199–2211. https://doi.org/10.1002/2017WR021692

Döpper, V., Jagdhuber, T., Holtgrave, A.-K., Heistermann, M., Francke, T., Kleinschmit, B., & Förster, M. (2022). Following the cosmic-ray-neutron-sensing-based soil moisture under grassland and forest: Exploring the potential of optical and SAR remote sensing. *Science of Remote Sensing*, *5*, 100056. https://doi.org/10.1016/j.srs.2022.100056

Evans, J. G., Ward, H. C., Blake, J. R., Hewitt, E. J., Morrison, R., Fry, M., et al. (2016). Soil water content in southern England derived from a cosmic-ray soil moisture observing system—COSMOS-UK. *Hydrological Processes*, *30*(26), 4987–4999. https://doi.org/10.1002/hyp.10929

Fersch, B., Francke, T., Heistermann, M., Schrön, M., Döpper, V., Jakobi, J., et al. (2020). A dense network of cosmic-ray neutron sensors for soil moisture observation in a highly instrumented pre-Alpine headwater catchment in Germany. *Earth System Science Data*, *12*(3), 2289–2309. https://doi.org/10.5194/essd-12-2289-2020

Fersch, B., Jagdhuber, T., Schrön, M., Völksch, I., & Jäger, M. (2018). Synergies for soil moisture retrieval across scales from airborne polarimetric SAR, cosmic ray neutron roving, and an in situ sensor network. *Water Resources Research*, *54*(11), 9364–9383. https://doi.org/10.1029/2018wr023337

Finkenbiner, C. E., Franz, T. E., Gibson, J., Heeren, D. M., & Luck, J. (2019). Integration of hydrogeophysical datasets and empirical orthogonal functions for improved irrigation water management. *Precision Agriculture*, *20*(1), 78–100. https://doi.org/10.1007/s11119-018-9582-5

Flynn, K. D., Wyatt, B. M., & McInnes, K. J. (2021). Novel cosmic ray neutron sensor accurately captures field-scale soil moisture trends under heterogeneous soil textures. *Water*, *13*(21), 3038. https://doi.org/10.3390/w13213038

Franz, T., Larios, A., & Victor, C. (2022). The bleeps, the sweeps, and the creeps: Convergence rates for dynamic observer patterns via data assimilation for the 2D Navier–Stokes equations. *Computer Methods in Applied Mechanics and Engineering*, *392*(15), 1–22. https://doi.org/10.1016/J.CMA.2022.114673

Franz, T. E., Wang, T., Avery, W., Finkenbiner, C., & Brocca, L. (2015). Combined analysis of soil moisture measurements from roving and fixed cosmic ray neutron probes for multiscale real-time monitoring. *Geophysical Research Letters*, *42*(9), 3389–3396. https://doi.org/10.1002/2015gl063963

Gianessi, S., Polo, M., Stevanato, L., Lunardon, M., Francke, T., Oswald, S., et al. (2022). Testing a novel sensor design to jointly measure cosmic-ray neutrons, muons and gamma rays for non-invasive soil moisture estimation. *Geoscientific Instrumentation, Methods and Data Systems Discussion*. (preprint) in review. https://doi.org/10.5194/gi-2022-20

Gibson, J., & Franz, T. E. (2018). Spatial prediction of near surface soil water retention functions using hydrogeophysics and empirical orthogonal functions. *Journal of Hydrology*, *561*, 372–383. https://doi.org/10.1016/j.jhydrol.2018.03.046

Greacen, E. L. (1981). *Soil water assessment by the neutron method*. CSIRO. https://doi.org/10.1016/j.jhydrol.2018.03.046

Heidbüchel, I., Güntner, A., & Blume, T. (2016). Use of cosmic-ray neutron sensors for soil moisture monitoring in forests. *Hydrology and Earth System Sciences*, *20*(3), 1269–1288. https://doi.org/10.5194/hess-20-1269-2016

Heistermann, M., Bogena, H., Francke, T., Güntner, A., Jakobi, J., Rasche, D., et al. (2022). Soil moisture observation in a forested headwater catchment: Combining a dense cosmic-ray neutron sensor network with roving and hydrogravimetry at the TERENO site Wüstebach. *Earth System Science Data*, *14*(5), 2501–2519. https://doi.org/10.5194/essd-14-2501-2022

Heistermann, M., Francke, T., Schrön, M., & Oswald, S. E. (2021). Spatio-temporal soil moisture retrieval at the catchment scale using a dense network of cosmic-ray neutron sensors. *Hydrology and Earth System Sciences*, *25*(9), 4807–4824. https://doi.org/10.5194/hess-25-4807-2021

Huisman, J. A., Hubbard, S. S., Redman, J. D., & Annan, A. P. (2003). Measuring soil water content with ground penetrating radar: A review. *Vadose Zone Journal*, *2*(4), 476–491. https://doi.org/10.2136/vzj2003.4760

Iwema, J., Schrön, M., Koltermann Da Silva, J., Schweiser De Paiva Lopes, R., & Rosolem, R. (2021). Accuracy and precision of the cosmic-ray neutron sensor for soil moisture estimation at humid environments. *Hydrological Processes*, *35*(11), e14419. https://doi.org/10.1002/hyp.14419

Ižvolt, L., Dobeš, P., & Ižbeta, P. (2016). Monitoring of moisture changes in the construction layers of the railway substructure body and its subgrade. *Procedia Locomotiveering*, *161*, 1049–1056. https://doi.org/10.1016/j.proeng.2016.08.847

Jagdhuber, T., Fersch, B., Schron, M., Jager, M., Voormansik, K., & Lopez-Martinez, C. (2018). Field-scale assessment of multi-sensor soil moisture retrieval under grassland. In *IGARSS 2018—2018 IEEE international geoscience and remote sensing symposium* (pp. 6111–6114). IEEE. https://doi.org/10.1109/IGARSS.2018.8517560

Jakobi, J., Huisman, J. A., Köhli, M., Rasche, D., Vereecken, H., & Bogena, H. R. (2021). The footprint characteristics of cosmic ray thermal neutrons. *Geophysical Research Letters*, *48*(15), e2021GL094281. https://doi.org/10.1029/2021GL094281

Jakobi, J., Huisman, J. A., Schrön, M., Fiedler, J., Brogi, C., Vereecken, H., & Bogena, H. R. (2020). Error estimation for soil moisture measurements with cosmic ray neutron sensing and implications for rover surveys. *Frontiers in Water*, *2*. https://doi.org/10.3389/frwa.2020.00010

Köhli, M., Schrön, M., & Schmidt, U. (2018). Response functions for detectors in cosmic ray neutron sensing. *Nuclear Instruments and Methods in Physics Research Section A: Accelerators, Spectrometers, Detectors and Associated Equipment*, *902*, 184–189. https://doi.org/10.1016/j.nima.2018.06.052

Köhli, M., Schrön, M., Zacharias, S., & Schmidt, U. (2023). *URANOS v1.0—The ultra rapid adaptable neutron-only simulation for environmental research*. Geoscientific Model Development Discussions, 16, 449–477. https://doi.org/10.5194/gmd-16-449-2023

Köhli, M., Schrön, M., Zreda, M., Schmidt, U., Dietrich, P., & Zacharias, S. (2015). Footprint characteristics revised for field-scale soil moisture monitoring with cosmic-ray neutrons. *Water Resources Research*, *51*(7), 5772–5790. https://doi.org/10.1002/2015wr017169

Köhli, M., Weimar, J., Schrön, M., Baatz, R., & Schmidt, U. (2021). Soil moisture and air humidity dependence of the above-ground cosmic-ray neutron intensity. *Frontiers in Water*, *2*, 66. https://doi.org/10.3389/frwa.2020.544847

Kouzes, R. T., Ely, J. H., Seifert, A., Siciliano, E. R., Weier, D. R., Windsor, L. K., et al. (2008). Cosmic-ray-induced ship-effect neutron measurements and implications for cargo scanning at borders. *Nuclear Instruments and Methods in Physics Research Section A: Accelerators, Spectrometers, Detectors and Associated Equipment*, *587*(1), 89–100. https://doi.org/10.1016/j.nima.2007.12.031

LGB (Landesamt für Geologie und Bergwesen) Sachsen-Anhalt. (2021). Retrieved from https://lagb.sachsen-anhalt.de/geologie/bodenkunde/fachinformationen-boden/bodenkarten/

McJannet, D., Hawdon, A., Baker, B., Renzullo, L., & Searle, R. (2017). Multiscale soil moisture estimates using static and roving cosmic-ray soil moisture sensors. *Hydrology and Earth System Sciences*, *21*(12), 6049–6067. https://doi.org/10.5194/hess-21-6049-2017

Meyer, R., Zhang, W., Kragh, S. J., Andreasen, M., Jensen, K. H., Fensholt, R., et al. (2022). Exploring the combined use of SMAP and Sentinel-1 data for downscaling soil moisture beyond the 1 km scale. *Hydrology and Earth System Sciences*, *26*(13), 3337–3357. https://doi.org/10.5194/hess-26-3337-2022

Patil, A., Fersch, B., Hendricks Franssen, H.-J., & Kunstmann, H. (2021). Assimilation of cosmogenic neutron counts for improved soil moisture prediction in a distributed land surface model. *Frontiers in Water*, *3*. https://doi.org/10.3389/frwa.2021.729592

Peng, J., Albergel, C., Balenzano, A., Brocca, L., Cartus, O., Cosh, M. H., et al. (2021). A roadmap for high-resolution satellite soil moisture applications—Confronting product characteristics with user requirements. *Remote Sensing of Environment*, *252*, 112162. https://doi.org/10.1016/j.rse.2020.112162

Rasche, D., Köhli, M., Schrön, M., Blume, T., & Güntner, A. (2021). Towards disentangling heterogeneous soil moisture patterns in cosmic-ray neutron sensor footprints. *Hydrology and Earth System Sciences*, *25*(12), 6547–6566. https://doi.org/10.5194/hess-25-6547-2021

Robinson, D. A., Campbell, C. S., Hopmans, J. W., Hornbuckle, B. K., Jones, S. B., Knight, R., et al. (2008). Soil moisture measurement for ecological and hydrological watershed-scale observatories: A review. *Vadose Zone Journal*, *7*(1), 358–389. https://doi.org/10.2136/vzj2007.0143

Rossel, R. A. V., Adamchuk, V. I., Sudduth, K. A., McKenzie, N. J., & Lobsey, C. (2011). Proximal soil sensing: An effective approach for soil measurements in space and time. In *Advances in agronomy* (1st ed., Vol. 113, pp. 243–291). Elsevier/Academic Press. https://doi.org/10.1016/B978-0-12-386473-4.00005-1

Schattan, P., Baroni, G., Oswald, S. E., Schober, J., Fey, C., Kormann, C., et al. (2017). Continuous monitoring of snowpack dynamics in alpine terrain by aboveground neutron sensing. *Water Resources Research*, *53*(5), 3615–3634. https://doi.org/10.1002/2016WR020234

Schattan, P., Köhli, M., Schrön, M., Baroni, G., & Oswald, S. E. (2019). Sensing area-average snow water equivalent with cosmic-ray neutrons: The influence of fractional snow cover. *Water Resources Research*, *55*(12), 10796–10812. https://doi.org/10.1029/2019WR025647

Schrön, M., Köhli, M., Scheiffele, L., Iwema, J., Bogena, H. R., Lv, L., et al. (2017). Improving calibration and validation of cosmic-ray neutron sensors in the light of spatial sensitivity. *Hydrology and Earth System Sciences*, *21*(10), 5009–5030. https://doi.org/10.5194/hess-21-5009-2017

Schrön, M., Köhli, M., & Zacharias, S. (2023). Signal contribution of distant areas to cosmic-ray neutron sensors—Implications for footprint and sensitivity. *Hydrology and Earth System Sciences*, *27*(3), 723–738. https://doi.org/10.5194/hess-27-723-2023

Schrön, M., Oswald, S. E., Zacharias, S., Kasner, M., Dietrich, P., & Attinger, S. (2021). Neutrons on rails: Transregional monitoring of soil moisture and snow water equivalent. *Geophysical Research Letters*, *48*(24), e2021GL093924. https://doi.org/10.1029/2021gl093924

Schrön, M., Rosolem, R., Köhli, M., Piussi, L., Schröter, I., Iwema, J., et al. (2018). Cosmic-ray neutron rover surveys of field soil moisture and the influence of roads. *Water Resources Research*, *54*(9), 6441–6459. https://doi.org/10.1029/2017wr021719

Schrön, M., Zacharias, S., Womack, G., Köhli, M., Desilets, D., Oswald, S. E., et al. (2018). Intercomparison of cosmic-ray neutron sensors and water balance monitoring in an urban environment. *Geoscientific Instrumentation, Methods and Data Systems*, *7*(1), 83–99. https://doi.org/10.5194/gi-7-83-2018

Stadt Blankenburg (Harz) (2021). Umweltbericht nach Umweltprüfung zum Bebauungsplan Nr. 19/21. In *"Stukenbreite," Fassung: Vorentwurf stand: Mai 2021*.

Stevanato, L., Baroni, G., Cohen, Y., Fontana, C. L., Gatto, S., Lunardon, M., et al. (2019). A novel cosmic-ray neutron sensor for soil moisture estimation over large areas. *Agriculture*, *9*(9), 202. https://doi.org/10.3390/agriculture9090202

Stevanato, L., Baroni, G., Oswald, S. E., Lunardon, M., Mares, V., Marinello, F., et al. (2022). An alternative incoming correction for cosmic-ray neutron sensing observations using local muon measurement. *Geophysical Research Letters*, *49*(6), e2021GL095383. https://doi.org/10.1029/2021GL095383

Topp, G. C., Davis, J. L., & Annan, A. P. (1980). Electromagnetic determination of soil water content: Measurements in coaxial transmission lines. *Water Resources Research*, *16*(3), 574–582. https://doi.org/10.1029/WR016i003p00574

UFZ, Helmholtz Centre for Environmental Research—UFZ. (2022). Drought monitor Germany. Retrieved from https://www.ufz.de/index.php?en=37937

Weimar, J., Köhli, M., Budach, C., & Schmidt, U. (2020). Large scale boron-lined neutron detection systems as a 3He alternative for cosmic ray neutron sensing. *Frontiers in Water*, *2*. https://doi.org/10.3389/frwa.2020.00016

Wieser, A., Güntner, A., Dietrich, P., Handwerker, J., Khordakova, D., Ködel, U., et al. (2022). First implementation of a new cross-disciplinary observation strategy for heavy precipitation events from formation to flooding. *Hydrology and Earth System Sciences Discussions*. (preprint) in review. https://doi.org/10.5194/hess-2022-131

Zink, M., Samaniego, L., Kumar, R., Thober, S., Mai, J., Schafer, D., & Marx, A. (2016). The German drought monitor. *Environmental Research Letters*, *11*(7), 074002. https://doi.org/10.1088/1748-9326/11/7/074002

Zreda, M., Desilets, D., Ferré, T. P. A., & Scott, R. L. (2008). Measuring soil moisture content non-invasively at intermediate spatial scale using cosmic-ray neutrons. *Geophysical Research Letters*, *35*(21), L21402. https://doi.org/10.1029/2008gl035655

Zreda, M., Shuttleworth, W. J., Zeng, X., Zweck, C., Desilets, D., Franz, T., & Rosolem, R. (2012). COSMOS: The COsmic-ray soil moisture observing system. *Hydrology and Earth System Sciences*, *16*(11), 4079–4099. https://doi.org/10.5194/hess-16-4079-2012